Power Harvesting and Telemetry in CMOS for Implanted Devices

Christian Sauer, *Student Member, IEEE*, Milutin Stanaćević, *Student Member, IEEE*, Gert Cauwenberghs, *Senior Member, IEEE*, and Nitish Thakor, *Fellow, IEEE*

Abstract—Implanted sensors offer many advantages to study and monitor the human body. Wires or batteries often compromise their usefulness. We describe a telemetry chip that by inductive coupling supplies power to and transmits digital data from an implantable sensor. The same two coils are used to transmit both power and data. The chip fabricated in 0.5-μm CMOS technology supplies 1.7 mA at 3.3 V, over a distance up to 25 mm between coils. Experiments emulating the effect of human tissue by introducing water bearing colloids between the two coils revealed a negligible loss of transfer efficiency. With modified Miller encoding, the data link attained $3 \ 10^{-5}$ `bit error rate` at 10 kbps transmission speed over 25 mm distance. Repeated tests using the same colloids between coils resulted in a slight decrease in the signal to noise ratio of the data stream with increasing thickness.

Index Terms—Biological interference, inductive powering, neural implants, radio frequency identification (RFID), transcutaneous link.

I. INTRODUCTION

AMONG the common applications of implanted microdevices are microelectrodes for electrical and chemical neural recording. Such recordings are often used by surgeons to both diagnose and determine treatment for brain disorders. In order to obtain sufficient power to amplify and record weak electrical signals, most electrodes are interfaced with wires connected through the skin. Unfortunately, this wiring or tethering limits the recording range in awake, behaving animals in chronic studies. Many studies have shown that there are physical changes in animal neurological structures when movement is restricted [1], [2]. In fact, studies have shown that animals can recover faster from brain injuries if they are in an environment that allows exploration and locomotion [3], [4].

One solution to this problem is the use of an active telemetry device packaged with a small battery. The major drawback of this solution is that the battery can not be fully implanted in the skull. The smallest batteries capable of powering an active sensor/transmitter combination are still too large for cranial implantation. Instead, an external carrying device is usually fit to the animal. There are several commercial implementations of this idea for behavioral recordings in live animals. While this solves the mobility problem, it still requires a hole through the epidermis. Any opening in the epidermal layer is a possible site for a major infection [5], [6]. A review of research into this area can be found in [7]. Rather than burden the animal with an external battery pack we have turned to energy harvesting.

Energy harvesting uses the external environment as a source of energy (e.g., temperature gradients, wind). For example, devices such as Smart Dust distributed networks make use of many different types of transducers, from solar power to vibration transducers [8]. Unfortunately, most of these types of energy gathering methods are unsuitable for a device implanted in the human body. A very promising alternative for implanted devices is radio frequency (RF) power harvesting through inductive coupling [9], [10]. In addition to gathering power, this technology can also be used to send data from the implant back to the base station, creating a two-way link [11]–[16]. The principles of the technique are the same as those behind the increasingly common RF identification (RFID) tags [17].

First conceived in the 1970's, these devices use inductive coupling to read an encoded identification sequence stored in the tag's memory and then report the value to the interrogator. Many applications exist for these devices, and millions of RFID tags have been sold. The first biological applications of these devices used them to keep track of animals (livestock). An RFID tag would be implanted in an animal and contain information about that animal that could then be read with the appropriate hardware. Later that same technology began to be used with sensors rather than static memories [18].

We have developed a power harvesting microchip based on this technique (Fig. 1) [19]. The device is designed to provide power, control signals, and a data link for an accompanying sensor to function. The chip can be utilized with many different types of sensors. Previous studies have shown that RF energy between 1 and 10 MHz penetrates the body with minimum energy loss [20]. To take advantage of this biological characteristic, we have designed our inductive link to operate at a frequency of 4 MHz. A transponder coil of 1 cm radius is used to receive power from the reader coil with a 2.5 cm radius. In this implementation, the chip supplies up to 2 mA at 3.3 V. In addition, it can be configured to supply various clocks and reference voltages necessary for the proper operation of the sensor. The chip is also designed to allow data transmission back to the module that broadcasts the power, removing any need for a physical connection.
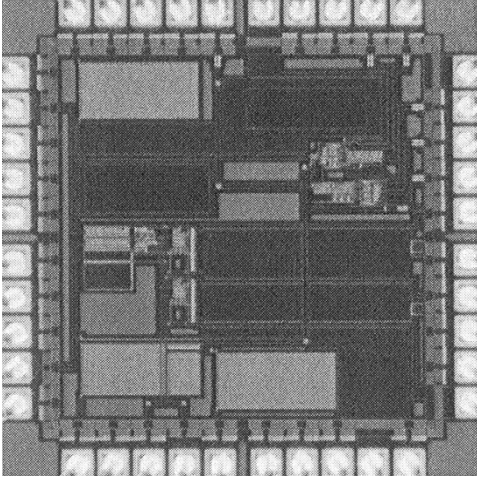
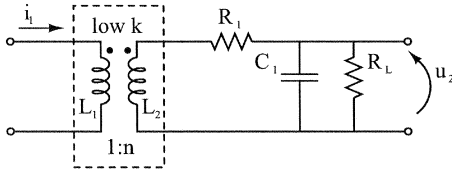Fig. 1. Photomicrograph of the fabricated chip.

Fig. 2. Simplified model of the inductively coupled system.

Transmission has been tested with two types of data encoding. Bit error rates (BERs) below $3 \cdot 10^{-5}$ at transmission speeds up to 10 kilobits per second (kbps) are measured and reported. We have also looked at the nonair coupling situation, in which there is a medium other than air between the coils.

II. INDUCTIVE COUPLING THEORY

Inductive coupling uses two inductor coils placed relatively close to one another. A primary coil is driven with a RF amplifier to create an electromagnetic field. The second coil, on the implanted device, captures a portion of this field. This induces a current through this secondary coil. The proportion of energy captured by the secondary coil can be represented by the coupling factor, k. This value (dimensionless and always between 0 and 1) is an important factor in the operation of any inductively coupled system. Typical values for k in inductively powered system are between 0.01 and 0.1.

The basic principles behind transferring power and data through an inductive link are the same as those used in transformer circuits. The major difference here is that in this case the two coils are fairly weakly coupled. The coupling factor between the two coils can be determined for the air coupling case empirically [17]

$$ k = \frac{r_{\text{implant}}^2 r_{\text{reader}}^2}{\sqrt{r_{\text{implant}} r_{\text{reader}}} \left(\sqrt{x^2 + r_{\text{reader}}^2} \right)^3}. \tag{1} $$

Equation (1) is based on the radii of the two coils and the distance x, between them. This equation assumes the two coils are parallel and center aligned, with only air between the two coils. While not as accurate as finite element modeling, this still provides a decent idea of the system coupling coefficient. This value
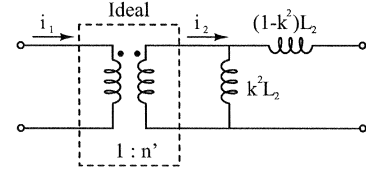

Fig. 3. Common model of a weakly coupled transformer.

TABLE I
SYSTEM SPECIFICATIONS

Parameter	L_1	L_2	C_1	R_1	R_L	ω
Value	43.5µH	3.7µH	330pF	1Ω	1k Ω	2π*4MHz

can then be used in a simplified model of the complete inductively coupled system shown in Fig. 2. The left side of this model represents the outside components of the system, while the right side includes a basic model of the implanted system. Here, R_1 represents the parasitic resistance in the coil, C_1 is the tuning capacitance used to raise the coil voltage, and R_L is the load on the system. The weakly coupled transformer is used here to represent the two discrete coils, L_1 and L_2. The primary coil, L_1, is driven by an RF amplifier supplying current i_1 at frequency ω. In the real system, R_L is time varying and complex. In this model it is represented as a real resistor. To proceed further, this weakly coupled transformer can be replaced by a common approximation (Fig. 3). In this model, the new ratio n' is given by

$$ n' = k \sqrt{\frac{L_2}{L_1}}. \tag{2} $$

According to the basic equations governing ideal transformer behavior, the current out of the transformer shown in Fig. 3 is

$$ i_2 = \frac{i_1}{n'}. \tag{3} $$

With a low coupling coefficient k, the impedance seen by current i_2 is approximately equal to that of an inductor with value $k^2 L_2$ (the impedance of this inductor is much lower than that of the other inductor in the circuit, nearly all of the current will flow through this inductor). Using the impedance equation of the inductor at a known frequency, the voltage induced by this current is

$$ u_T = j\omega L_2 k^2 \left(\frac{i_1}{n'} \right) $$
$$ = j\omega L_2 k^2 \left(i_1 \frac{1}{k} \sqrt{\frac{L_1}{L_2}} \right) $$
$$ = j\omega k \sqrt{L_1 L_2} i_1 \tag{4} $$

where u_T is the voltage across the L_2 component of the transformer induced by the current i_1. We can now replace the weakly coupled transformer in Fig. 2 with a voltage source, u_T, in series with an inductor. With a small k value, we can approximate the value of this inductor by L_2. In this simplified case, a basic equation for the voltage across the load, u_2, is given by

$$ u_2 = \frac{u_T}{1 + (j\omega L_2 + R_1) \left(\frac{1}{R_L} + j\omega C_1 \right)}. \tag{5} $$

Equation (5) makes use of the impedances of the various components at a known frequency of operation. Substituting in the equation for the transformer voltage (4) and solving for the real
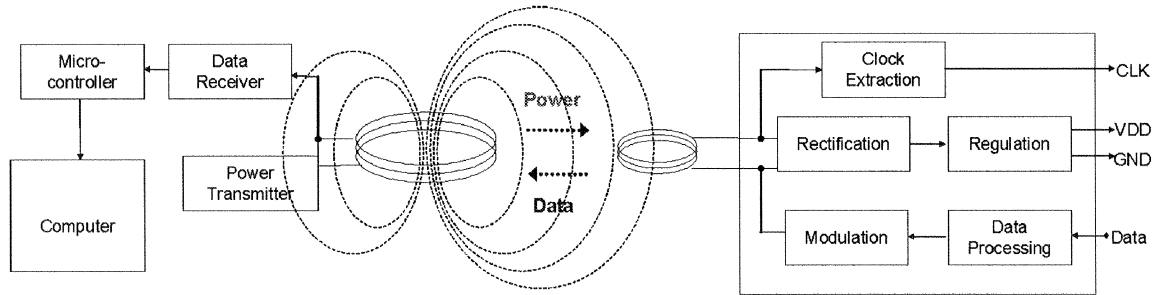
Fig. 4. Block diagram of the telemetry system.

part of the solution leads to a final answer with respect to the known parameters of the system

$$u_2 = \frac{\omega\,k\sqrt{L_1 L_2}\,i_1}{\sqrt{\left(\frac{\omega L_2}{R_L} + \omega R_1 C_1\right)^2 + \left(1 - \omega^2 L_2 C_1 + \frac{R_1}{R_L}\right)^2}}. \quad (6)$$

In the specific case we are interested in, our choices in coil sizes have led to the system parameters given in Table I.

This creates a linear scale factor A, the gain of the system, with units of ohms. For this system, A is approximately a factor of 1270 Ω. The new equation for this particular system becomes

$$u_2 = 1270\,\Omega\,k\,i_1 \quad (7)$$

where we require u_2 within a certain range and k is a factor of the distance between the two coils. Therefore, by changing the current through the primary coil of the system the voltage on the implanted coil could be adjusted for a fixed coupling factor. This gives a required coil (rms) current on the order of 100 mA for the system with weak coupling. This gives a target for the further design of components in the system, which can lead to further iterations with these equations with different parameters.

III. ARCHITECTURE

As shown in the system diagram (Fig. 4), the chip consists of several subunits: rectifier, regulator, voltage bias, clock recovery, and data encoder. The transmission coil voltage is driven by a high efficiency Class-E transmitter. The sinusoidal voltage on the receiver coil is dependant on the geometry of the coils. A full-wave rectifier followed by a low pass filter recovers a dc voltage. This voltage is dependent on the load and is not suitable for powering active circuitry.

A voltage regulator module reduces this voltage and holds it approximately constant regardless of current draw. The value of the constant voltage is set using a voltage reference circuit; this block generates a reference voltage independent of the voltage in the coil (as long as it exceeds a minimum value). We used separate analog and digital regulators on the microchip to avoid noise from the digital circuitry interfering with the more sensitive analog components. The entire analog system dissipates 35 μW.

A clock is recovered from the input sine wave. This allows the sensor to be synchronized with the transmitter and removes the need for an on-chip oscillator. Data [in nonreturn-to-zero (NRZ) format] is taken in for encoding and transmission to the base station. The data is encoded into a more energy-efficient format for broadcasting. Transmission is accomplished through the same
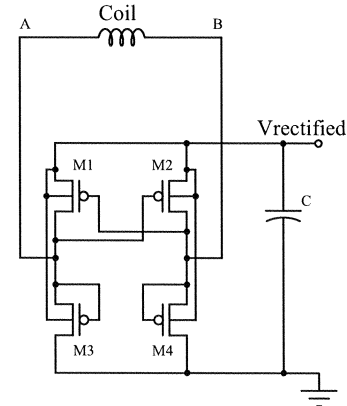

Fig. 5. Rectifier circuit diagram.

coil used to capture voltage. By modifying the impedance of this transponder coil it is possible to transmit data efficiently. The change in implanted coil impedance modulates the amount of current through the transmission coil. This change can be read out with a current sensor and envelope detector at the transmission station. The received signal can then be decoded and acquired.

A. Rectifier

The rectifier circuit is a full wave rectifier composed of four pMOS transistors (Fig. 5) [21]. Bipolar junction transistors (BJTs) and diodes, while somewhat feasible in a commercial CMOS process, do not have good characteristics (i.e., low betas and high leakage) and are avoided. When voltage on side A of the coil is higher than that of side B, M2, and M3 are shut off while M1 and M4 are turned on. This ties the low voltage side of the coil to ground while passing the high voltage. The situation is reversed when B is higher than A. The use of pMOS transistors prevents latch-up inducing collector currents from occurring and removes the necessity of using additional components.

The resulting output is passed through an *RC* filter with an external capacitor. By properly sizing the pMOS transistors the voltage drop across the rectifier is minimized and the rectified voltage is close to the root-mean-square (rms) voltage of the received sine wave. For an output voltage of 3.3 V, a voltage amplitude of at least 7 V is required to be present on the coil (a 4.9 V rms voltage). A standard CMOS process has a transistor gate break down voltage of 12 V, effectively setting an upper limit on the received voltage. The circuitry can be protected through the use of an off chip Zener diode, although it
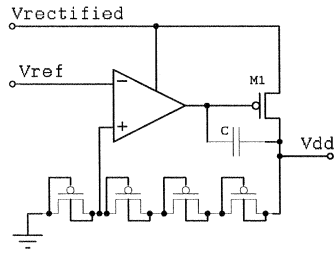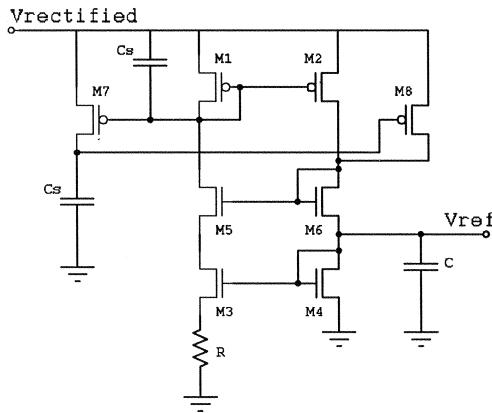
Fig. 6. Regulator circuit diagram.

Fig. 7. Voltage reference circuit.

introduces certain parasitic capacitance that must to be taken into account. Unfortunately, this parasitic capacitance mainly affects the circuit when the diodes are in operation. Such transient capacitance can not be compensated with normal methods and creates a discontinuity in circuit operation.

B. Regulator

The regulator circuit produces a steady 3.3 V output and can supply upwards of 2 mA (depending on the transmitted power). The circuit uses a transconductance amplifier to control the gate of a large pMOS transistor (M1 in Fig. 6). Through negative feedback, the output voltage is stabilized at a voltage proportional to the voltage reference. A series of resistively connected pMOS allow the reference voltage to be one quarter of the required output voltage while consuming a small amount of power. A feedback capacitor between the gate of the transistor and the output ensures system stability. A current draw of $100\,\mu\text{A}$ is necessary to keep the system operating in the proper regime.

C. Voltage Reference

The regulator requires a voltage reference to set the voltage output independently of the received power. The system is designed for implantation in the human body. A consequence is that the temperature of the implant will be held constant. This avoids the use of a bandgap reference circuit (which would require BJTs). Instead, we have made use of a current bias circuit that allows a supply independent reference to be generated using only standard CMOS devices (Fig. 7). A startup circuit (M7 and M8) moves the circuit out of its quiescent state. This circuit is designed to produce an 800 mV reference voltage at body temperature, with less than 1% variation with the supply [22].
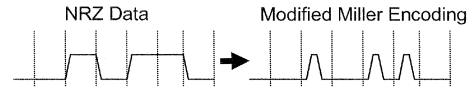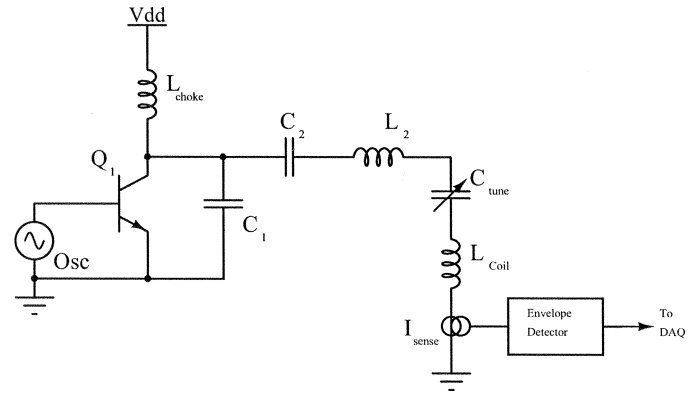

Fig. 8. Data encoding characteristics.

Fig. 9. Base station schematic.

D. Clock Recovery

A 4 MHz clock is recovered from the sinusoidal waveform in the coil. A chain of inverters recovers a digital signal. This signal, synchronized with the base station, can be used for extracting data from the sensor. In addition, some sensors may require several different clock frequencies different from 4 MHz. Slower clocks can be provided by dividing this clock frequency. In the initial version of the chip the 4 MHz carrier is divided down to a 1 MHz master clock.

E. Data Encoding and Modulation

Data is accepted from the sensor in NRZ format. The data is encoded in a modified Miller encoding scheme. For every logical one in the NRZ data stream a pulse is generated (Fig. 8). The pulsewidth is controlled by an input clock for ease of testing. This clock could also be supplied by one of the clocks generated on chip. This encoding format uses two transitions for every one, but none for a zero. Data transmission is accomplished by changing the value of the load resistor. A secondary resistor and nMOS transistor is connected between one of the coil terminals and the ground in series. The nMOS transistor is switch on or off based on the data value to be transmitted. This modulates the impedance of the coil, a change that can be read out on the transmission coil. The value of the resistor was chosen to be 500 Ohms as tradeoff between sensitivity in detecting the change at the reader and power dissipated on the resistor. With the modified Miller encoding scheme the amount of time that the resistor is in the circuit is minimized. This requires the modulation resistor to be on for a fraction of the time required by the NRZ data format, depending on the clock frequency chosen for the pulses. This scheme is also more tolerant to noise. It does not depend on the duration of a high pulse, but rather the occurrence of such a pulse. This allows more leeway in the decoding hardware, as delays and rise times are not as important to the recovery algorithm.

F. Power Transmitter and Data Recovery

A modified Class-E amplifier is used to drive the transmission coil and provide power for the system (Fig. 9). A Class-E ampli-
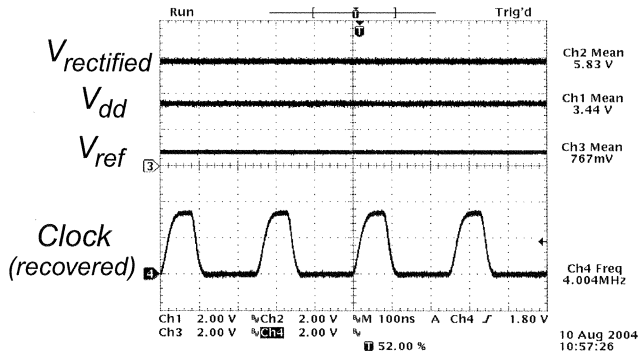
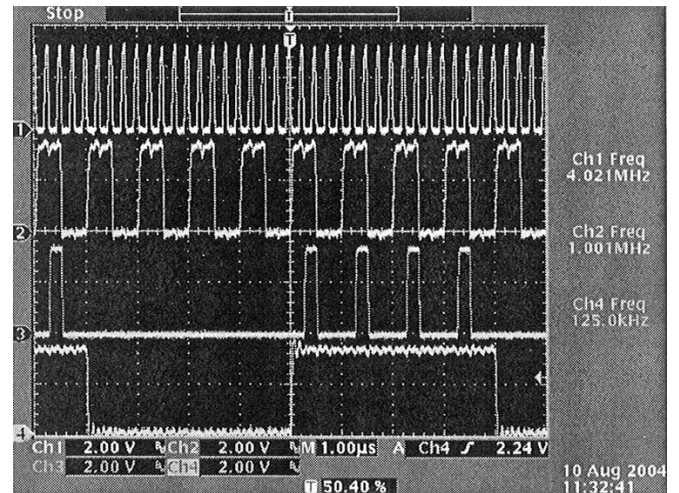Fig. 10.   Oscilloscope trace of the microchip analog waveforms.

Fig. 11.   Oscilloscope trace of the microchip digital waveforms. From the top the traces are the recovered clock (Ch1), the divided clock (Ch2), the encoded data (Ch3) and the input data (Ch4).
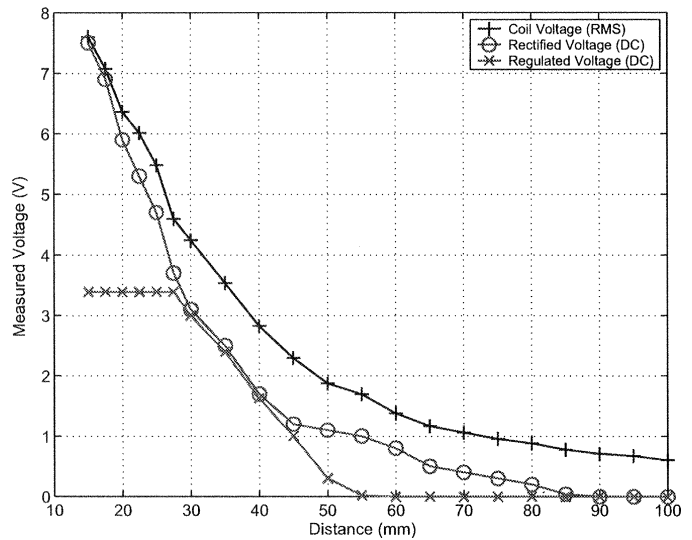

Fig. 12.   Air coupling at various distances.

fier is used because of its high efficiency and low power supply voltage requirement. In this case a variable supply voltage was used, ranging from 2.5 to 5 V. This allowed variable amounts of power transfer without changing coil sizes or positions. The system produces voltages as high as 300 V across the drive coil, with currents on the order of 300 mA. While high, these voltages are not dangerous because they are produced by a tuned *LC* circuit (tuned to various coil inductances through the use of the variable capacitor). If any exposed wiring comes into contact with another material (such as skin), the circuit will quickly detune and the high voltage will be lost. The current through the coil is converted to a voltage through a current sensing transformer. The voltage is then put through a rectifier and filtered to recover the envelope. A data acquisition card samples the voltage at the output of the envelope detector for further processing. The amplifier and data recovery circuit were realized with discrete components on a board separate from the microchip test circuitry.

IV. MEASUREMENT RESULTS

The chip has been fabricated in a 0.5-μm bulk CMOS process through the MOSIS foundry. In order to test the chip with inductive coupling, we used a Class-E transmitter. This circuit produced a high power RF signal at 4 MHz, using an antenna coil 5 cm in diameter that was used through all the experiments to power to chip. The diameter of the coil was chosen for maximum magnetic field at a read distance of 2 cm [17]. A similar but smaller coil (2 cm in diameter) was used to harvest the broadcast energy. The radius of the implanted coil was chosen as a tradeoff between maximizing the coupling coefficient (1) and size constraints. The coils were made as 'pancake' coils of copper magnet wire 0.56 mm in diameter. Based on values of inductances given in Table I, the reader coil had 17 turns and the implanted coil had 9 turns. The two components were realized on different prototyping boards, with isolated ground planes. A data acquisition card sampling at 50 kHz was used to sample the envelope of the voltage output of the current sensor on the transmitter to detect transmitted data. Fig. 10 illustrates the basic waveforms of the chip during operation. The largest voltage (Ch2) is the rectified voltage, followed by the regulated (Ch1) and than the reference (Ch3) voltages. The recovered 4 MHz clock (Ch4) is shown at the bottom of the trace. Fig. 11 shows the digital encoding behavior of the microchip, with the two on-chip clocks used in the encoder. The top trace is the recovered clock (Ch1), the second is the divided 1 MHz clock (Ch2), the third represents the Miller encoded data (Ch3), and the last is the data input to the system (Ch4).

A. Air Coupling at Various Distances

To test the coupling and determine the maximum power transfer the transmitter and receiver coils were placed close together and moved apart. As shown in Fig. 12, distances between 10 and 100 mm were tested. The chip was loaded such that it would produce 0.7 mA when the voltage was enough to operate the regulator. With this load the chip was able to provide the desired regulated voltage with a distance of up to 28 mm between the two coils. The rms voltage on the coil, the rectified voltage, and the regulated voltage were recorded. For the range of 3.8 to 7.4 V of the input voltage to the regulator, line regulation was measured to be 0.15%. At low current draw the rectified voltage follows the coil rms voltage fairly closely. The two values diverge when more current is drawn from the
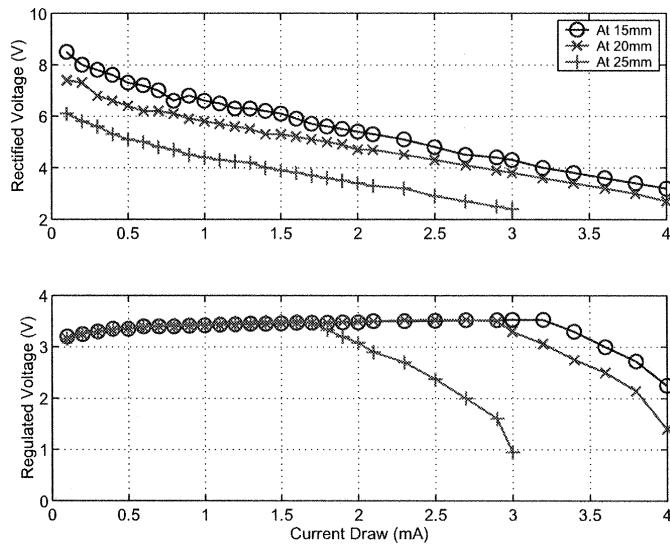
Fig. 13.   Load regulation.

Fig. 14.   Coupling losses due to medium layers.

regulator. When the rectified voltage drops to the regulated value, the pMOS controlling current is completely on. This ties the regulated voltage to the rectified, while affecting the coil voltage slightly less.

B. Load Regulation

The amount of current the chip could source before the regulator became inoperative was also tested (Fig. 13). The maximum current sourced depends on the distance between the two coils. The amount of voltage change until the drop off point was constant across all distances tested. This experiment was repeated several times at different distances, which changed the coupling factor and the maximum deliverable power. The chip has dual voltage regulators that can be used to supply both digital and analog sources (only the results for a one of these are shown, the second showed identical characteristics). Both voltages were designed to be 3.3 V. In tests these voltages were actually measured to be 3.4 and 3.5 V. The mismatch is due to mismatch between transistors in the regulator feedback pathway. The load regulation was measured to be 2.72%. The positive slope that occurred in this experiment is likely due to the increased gate voltage required by the larger current draw. With the large size of this device, the drain voltage has a small inverse dependence on the gate voltage. While slight enough to keep the system operating near the required point, it still affects the final voltage.

C. Coupling and Interference

The previous tests examine the characteristics of the system when only air exists between the two coils. However, as the device is intended to be implanted, this assumption is unrealistic. Biological tissue will obviously have some effect on the coupling between the two coils. While truly recreating biological tissue was beyond the scope of this investigation, we made use of the fact that the main component of the human body is water. We added water bearing colloid samples between the two coils. This allowed us to control the thickness of the sample without an elaborate setup. In addition, by controlling the amount of impurities in the gel (i.e., the salt content of the colloid) the con-
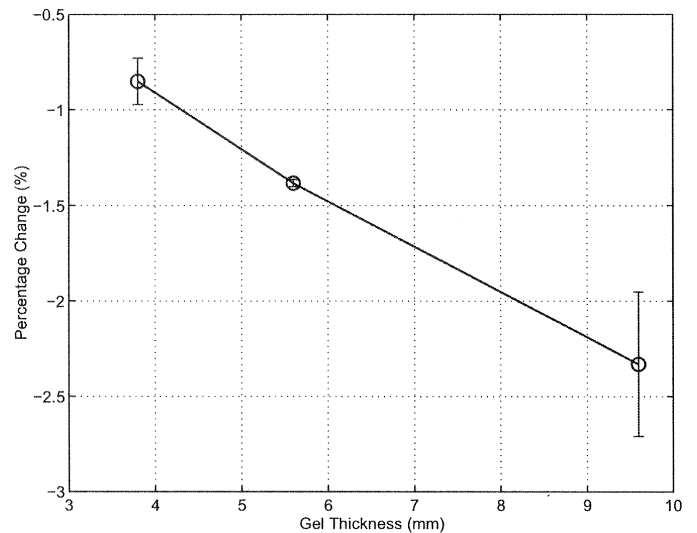
ductivity of the material could be varied [25]. The gels used had a density of .74 g/cm^2 and a conductivity of about 10 S/m, in excess of the expected average tissue conductivity. Simple tissue finite element models (FEMs) have revealed the similarity of such simple gels to more complex layered tissues, as long as the average conductivities of each are comparable.

The distance between the coils was held constant at 25 mm and the rms of the recovered voltage was measured. The results are shown in Fig. 14. The plot shows the percentage change from the base value (air coupling at 25 mm) when samples of different thickness are interposed between the two coils. Several measurements for each gel thickness were recorded. The results were varied (especially for large gel thicknesses), as can be seen from the Fig. 14. The general trend is a decrease in the amount of power transferred; however, this drop was never enough to reach the minimum operating voltage of the circuitry.

D. Data Transfer With Air Coupling

In order to determine the best scheme for transmitting data, NRZ data and modified Miller encoded data were sent through the data link at different rates. These experiments were performed under the normal operating conditions of the system (a load of 0.7 mA at a distance of 25 mm, the same as the previous set of experiments). In each case a random stream of bits was encoded and sent through the link for several seconds. In all cases 10 s of data were sent and recorded, resulting in at least 10^4 bits (for the slowest data rate) and at most 10^5 bits. Data transfer speeds between 1 and 10 kHz were tested. Higher speeds are possible with the integrated circuitry; the 10 kHz limitation in the current setup is due to the particular decoding scheme implemented off-chip at the receiver. Fig. 15 shows acquired data that was modified Miller encoded after it has been passed through the wireless link. At higher data transmission rates the signal is smaller and harder to detect. The envelope of the received signal was decoded into a binary string and compared with the original data. The results for all the tests are summarized in Table II.

Both types of data show that our system is capable of operation at frequencies up to 10 kHz. At the highest frequency errors
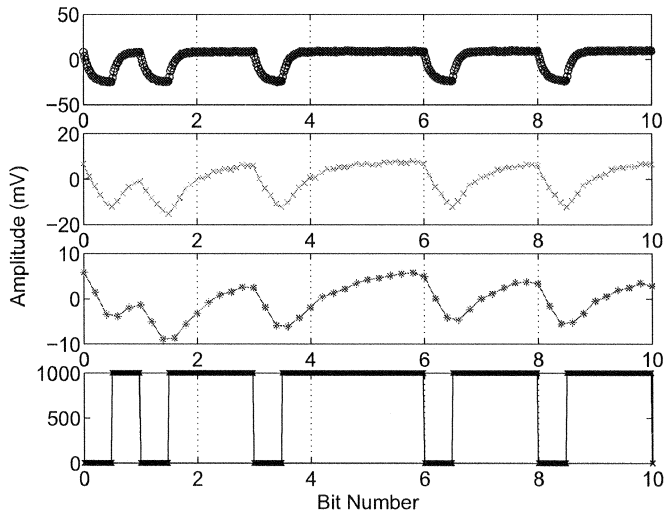
Fig. 15. Comparison of data envelopes at frequencies tested for the Miller encoded data stream '1 101 001 010'. From the top, data at 1 kbps, data at 5 kbps, data at 10 kbps, and the ideal output Miller encoded data.

Fig. 16. Data envelope with air coupling (x) and with 8 mm of gel between coils (o).

TABLE II
DATA TRANSFER TEST RESULTS

Encoding	Speed (kbs)	Bits Sent	Errors	BER
NRZ	1	$1*10^4$	0	0
	5	$5*10^4$	0	0
	10	10^5	168	$1.68*10^{-3}$
Modified Miller	1	$1*10^4$	0	0
	5	$5*10^4$	0	0
	10	10^5	3	$3*10^{-5}$

occur in both data formats. The greater prevalence of errors in the NRZ data is likely due to the increased complexity of decoding such data. While Miller data can be simply decoded by determining either up or down transitions of the signal, NRZ data relies on the precise timing of both types of transitions.

Modified Miller encoding has a major advantage over NRZ data. In a random signal, an NRZ signal will require the impedance modulating resistor to be linked to the coil for 50% of the transmission time. While on, this resistor dissipates power and lowers the rectified voltage. In our design, for the chosen value of the resistor of 500 Ω, the power dissipated on the resistor was equal to 20% of the power delivered. This reduces the efficiency of the system as a whole and can reduce the operating range (not to mention increasing the temperature of an implanted system). In contrast, the modified Miller encoding requires the resistor to be in the circuit for an average of 25% of the transmission time (with an encoding pulse width of half the data frequency).

In the expected application of our system, it is likely that data speed will not be as important as power consumption and operating range. We have thus chosen to continue with the modified Miller format in our design, accepting the increased circuitry complexity in return for fewer errors and better power efficiency.

E. Data Transfer With Biological Interference

As with the power transfer aspect of this project, it is important to understand the influence that a different medium between the two coils would have on the functionality of the system. To test this we again used both NRZ and modified Miller encoded
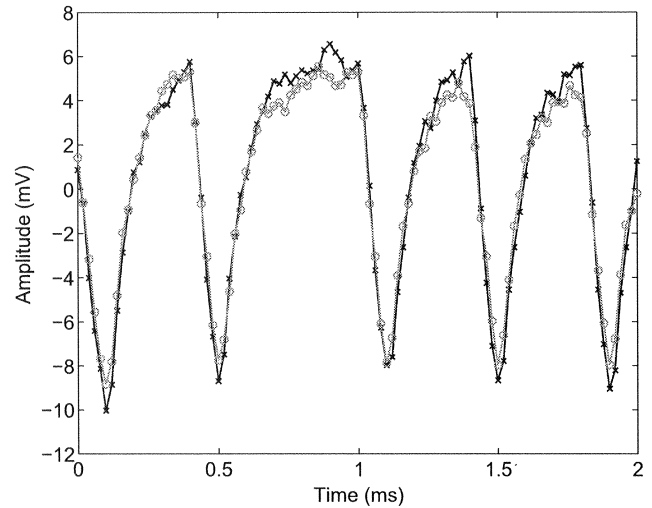
data. The frequency was kept at 5 kbps (a data transfer rate at which there were no errors in either type of data, as determined from the previous set of experiments). Gels of differing thicknesses (from 3 to 8 mm) were inserted between the two coils to determine the new error rates. As with the previous set of experiments, $5*10^4$ bits were sent and captured. Fig. 16 shows the differences in received data envelopes. The signal is attenuated by a slight amount in the case where it passes through the 8 mm thick gel ("o" in Fig. 16). With both data formats there were no errors introduced into the data streams for any gel thickness. These results track with those shown in power experiments. While there is certainly an attenuation of the signal, it is not great enough to cause a disruption in data or power flow. This attenuation is likely to be increasingly important at faster data speeds and should be taken into account when planning the final system characteristics.

V. APPLICATION

To test the application of this system we have chosen to use it to transfer electroencephalogram (EEG) data taken during animal recording (Fig. 17), taken during a previous set of experiments [23]. The data was first recorded and later transmitted through this data link. The recording of 4 channels of EEG was acquired at 125 Hz. The four channels were interleaved and sent at a 5 kbps data rate, using NRZ data encoding. The resulting data stream was read into the computer and reconstructed to display the original waveform. For this transmission (10^4 bits) there were no errors. The resulting signal was separated again into the four component channels, as shown in Fig. 17. The data represents recordings from four discrete electrodes (macro size) in a rat cortex. Such data is used to predict and analyze seizure behavior. This data consists not of spike recordings (from single or populations of neurons) but rather the electric field generated by many neurons. Typically used in many different types of analysis, such data has frequencies of interest in the region of 0.1–50 Hz, requiring a sampling rate of at least 100 Hz. Such data can be sampled at 10 bits, which at 5 kbps equates to four channels of data with some overhead for error detection.
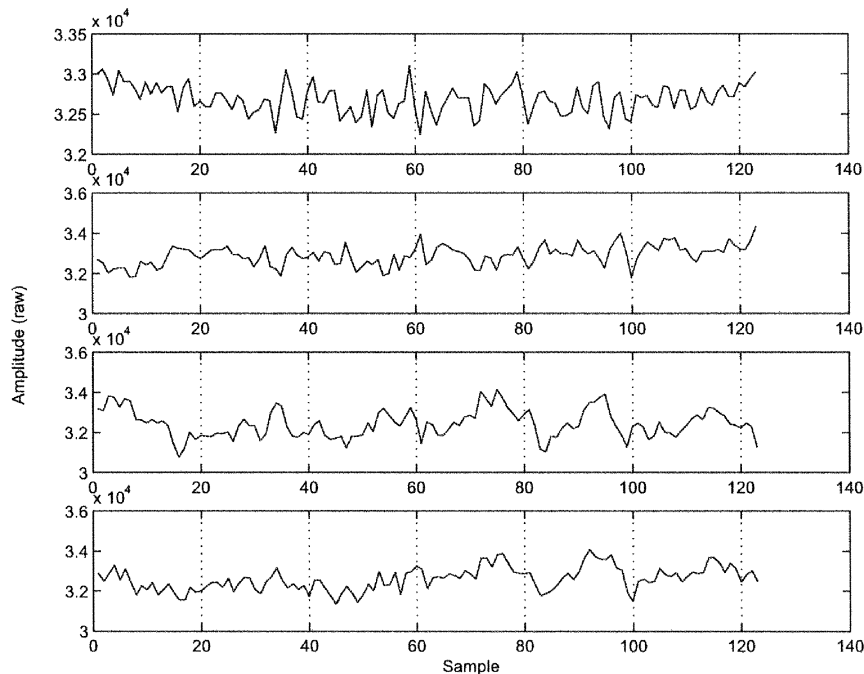
Fig. 17.   EEG data transferred across the telemetry system.

TABLE III
TELEMETRY SYSTEM CHARACTERISTICS

Process	0.5 μm, 3M2P Bulk CMOS
Active chip area	0.1 mm^2
Regulated voltage	3.4 V
Maximum power supplied	11 mW
Operating range (max load)	15 mm
Typical power supplied	2.4 mW
Operating range (typ. load)	28 mm
Maximum data transfer rate (receiver limited)	10 kbs

VI. DISCUSSION

We have presented the design and initial test results for a generic chip that can be used to power and interface with an implanted sensor. The chip has dual voltage regulators that can be used to supply both digital and analog sources. In addition to supplying power, the chip also provides a pathway to send data outside the body. To facilitate this, there exists encoding digital logic built into the chip to format the data. Tests have shown that using this encoding reduces the speed at which data can be read out from the chip. The major advantage to such encoding is the increased efficiency of the chip, reducing the power dissipation necessary to transmit data through the skin. Tests have shown that acceptable errors rates can be obtained with data transfer rates as great as 10 kbps, although a choice of 5 kbps ensures data integrity. The data rates shown are application specific and not limited by the integrated circuitry, but the particular data recovery circuits at the receiver. The characteristics of the chip are summarized in Table III and can be compared to characteristics of other inductive link circuits [13].

In future designs, we plan to implement a combined sensor and telemetry chip. This system will have everything necessary to record and transmit data on a single substrate. The final design will make use of advanced neurological monitoring circuitry [24]. This type of neurochemical monitoring circuitry has a relatively low sampling rate, matching well with the optimizations we have chosen for our system. In addition, we intend to study further the effect of interference between the two coils. Coil sizing is expected to play a major role in this dependency and we are currently performing FEM analysis of the intervening conductive media to determine the optimal coil sizes.

ACKNOWLEDGMENT

REFERENCES

[1] W. A. Van Gool, H. F. Pronker, M. Mirmiran, and H. B. Uylings, "Effect of housing in an enriched environment on the size of the cerebral cortex in young and old rats," *Exp. Neurol.*, vol. 96, no. 1, pp. 225–32, 1987.

[2] P. A. Ferchmin and E. L. Bennett, "Direct contact with enriched environment is required to alter cerebral weights in rats," *J. Comp. Physiol. Psychol.*, vol. 88, no. 1, pp. 360–7, 1975.

[3] A. Belayev, I. Saul, Y. Liu, W. Zhao, M. D. Ginsberg, M. A. Valdes, R. Busto, and L. Belayev, "Enriched environment delays the onset of hippocampal damage after global cerebral ischemia in rats," *Brain Res.*, vol. 964, no. 1, pp. 121–127, 2003.

[4] A. Risedal, B. Mattsson, P. Dahlqvist, C. Nordborg, T. Olsson, and B. B. Johansson, "Environmental influences on functional outcome after a cortical infarct in the rat," *Brain. Res. Bull.*, vol. 58, no. 3, pp. 315–321, 2002.

[5] B. E. Swartz, J. R. Rich, P. S. Dwan, A. DeSalles, M. H. Kaufman, G. O. Walsh, and A. V. Delgado-Escueta, "The safety and efficacy of chronically implanted subdural electrodes: A prospective study," *Epilepsy*, vol. 46, pp. 87–93, 1996.

[6] W. Lee, J. Lee, S. Lee, J. Kang, and T. Ko, "Complications and results of subdural grid electrode implantation in epilepsy surgery," *Surg. Neurol.*, vol. 54, pp. 346–51, 2000.

[7] P. Mohseni, K. Najafi, S. Eliades, and X. Wang, "Wireless multichannel biopotential recording using and integrated FM telemetry circuit," *IEEE Trans. Neural Syst. Rehab. Eng.*, vol. 13, no. 3, pp. 263–271, Jun. 2005, to be published.

[8] B. Warneke, B. Atwood, and K. S. Pister, "Preliminary smart dust mote," *Hot Chips*, vol. 12, no. 1, 2000.

[9] W. J. Heetderks, "RF powering of millimeter- and submillimeter-sized neural prosthetic implants," *IEEE Trans. Biomed. Eng.*, vol. 33, no. 3, pp. 323–327, Mar. 1988.

[10] M. Ghovanloo and K. Najafi, "Fully integrated wide-band high-current rectifiers for inductively powered devices," *IEEE J. Solid-State Circuits*, vol. 39, no. 9, pp. 1976–1984, Sep. 2004.

[11] P. Irazoqui-Pastor, I. Mody, and J. W. Judy, "In-vivo EEG recording using a wireless implantable neural transceiver," in *Proc. 1st Int. IEEE EMBS Conf. Neural Engineering*, vol. 1, 2003, pp. 622–625.

[12] A. D. DeHennis and K. D. Wise, "A wireless microsystem for the remote sensing of pressure, temperature, and relative humidity," *J. MEMS*, vol. 14, no. 1, pp. 12–22, 2005.

[13] M. Sawan, Y. Hu, and J. Coulombe, "Wireless smart implants dedicated to multichannel monitoring and microstimulation," *IEEE Circuits Syst. Mag.*, vol. 5, no. 1, pp. 21–39, Jan. 2005.

[14] W. Liu, K. Vichienchom, M. Clements, S. C. DeMarco, C. Hughes, E. McGucken, M. S. Humayun, E. De Juan, J. D. Weiland, and R. Greenberg, "A neuro-stimulus chip with telemetry unit for retinal prosthetic device," *IEEE J. Solid-State Circuits*, vol. 35, no. 7, pp. 1487–1497, Jul. 2000.

[15] T. Akin, K. Najafi, and R. M. Bradley, "A wireless implantable multichannel digital neural recording system for a micromachined sieve electrode," *IEEE J. Solid-State Circuits*, vol. 33, no. 1, pp. 109–118, Jan. 1998.

[16] M. Ghovanloo and K. Najafi, "A wide-band frequency-shift keying wireless link for inductively powered biomedical implants," *IEEE Trans. Circuits Syst. I, Reg. Papers*, vol. 51, no. 12, pp. 2374–2383, Dec. 2004.

[17] K. Finkenzeller, *RFID Handbook*. London, U.K.: Wiley, 2003.

[18] P. R. Troyk, "Injectable electronic identification, monitoring, and stimulation systems," *Annu. Rev. Biomed. Eng.*, vol. 1, pp. 177–209, 1999.

[19] C. Sauer, M. Stanacevic, G. Cauwenberghs, and N. Thakor, "Power harvesting and telemetry in CMOS for implanted devices," in *Proc. IEEE BioCAS Conf.*, vol. 1, 2004, pp. S1/8–S1-4.

[20] P. Vaillancourt, A. Djemouai, J. F. Harvey, and M. Sawan, "EM radiation behavior upon biological tissues in a radio-frequency power transfer link for a cortical visual implant," in *Proc. IEEE EMBS Conf.*, vol. 6, 1997, pp. 2499–2502.

[21] P. Rakers, L. Connell, T. Collins, and D. Russell, "Secure contactless smartcard ASIC with DPA protection," *IEEE J. Solid-State Circuits*, vol. 36, no. 3, pp. 559–565, Mar. 2001.

[22] T. Delbruck and A. van Schaik, "Bias current generators with wide dynamic range," in *Proc. ISCAS*, vol. 1, 2004, pp. 337–340.

[23] D. L. Sherman, M. K. Atit, R. G. Geocadin, S. Venkatesha, D. F. Hanley, A. L. Natarajan, and N. V. Thakor, "Diagnostic instrumentation for neurological injury," *IEEE Instrum. Meas. Mag.*, vol. 5, no. 2, pp. 28–34, Feb. 2002.

[24] K. Murari, N. Thakor, M. Stanacevic, and G. Cauwenberghs, "Wide-range, picoampere-sensitivity multichannel VLSI potentiostat for neurotransmitter sensing," in *Proc. EMBC*, vol. 2, 2004, pp. 4063–4066.

[25] E. Shapiro, A. Borthakur, M. Shapiro, R. Reddy, and J. Leigh, "Fast MRI of RF heating via phase difference mapping," *Magn. Reson. Med.*, vol. 47, pp. 492–498, 2002.

Christian Sauer (S'03) received the B.S. and the M.S. degrees in biomedical engineering from the Johns Hopkins University, Baltimore, MD, in 2003, and 2005, respectively.

He is currently working on commercial applications of biomedical VLSI circuits. His primary reasearch intrests include analog integrated circuits and their application to medical problems, with his research focused on developing circuitry for implantable neural probes.

Milutin Stanaćević (S'00) received the B.S. degree in electrical engineering from the University of Belgrade, Belgrade, Serbia and Montenegro, in 1999, and the M.S. and Ph.D. degrees in electrical and computer engineering from Johns Hopkins University, Baltimore, MD, in 2001 and 2005, respectively.

He is currently an Assistant Professor in the Department of Electrical and Computer Engineering, State University of New York, Stony Brook. His research interests include mixed-signal VLSI circuits, systems, and algorithms for parallel multi-channel sensory information processing with emphasis on real-time acoustic source localization and separation, and micropower implantable biomedical instrumentation and telemetry.

Gert Cauwenberghs (SM'89–M'94–S'03) received the Ph.D. degree in electrical engineering from California Institute of Technology, Pasadena, in 1994.

He was a Professor of Electrical and Computer Engineering at Johns Hopkins University, Baltimore, MD. He joined the University of California, San Diego as Professor of neurobiology in 2005. His research covers VLSI circuits, systems and algorithms for parallel signal processing, adaptive neural computation, adaptive optics, and biomedical instrumentation.

He received the National Science Foundation Career Award in 1997, the Office of Naval Research Young Investigator Award in 1999, and the White House PECASE Award in 2000. He serves as Associate Editor of the IEEE TRANSACTIONS ON CIRCUITS AND SYSTEMS—I : REGULAR PAPERS, and the IEEE SENSORS JOURNAL. He was Distinguished Lecturer of the IEEE Circuits and Systems Society and chaired its Analog Signal Processing Technical Committee.

Nitish V. Thakor (S'78–M'81–S'89–F'97) received the B. Tech. degree in electrical engineering from the Indian Institute of Technology (IIT) Bombay, Mumbai, India, in 1974, and the Ph.D. degree in electrical and computer engineering from the University of Wisconsin, Madison, WI, in 1981.

He served on the faculty of Electrical Engineering and Computer Science of the Northwestern University between 1981 and 1983, and since then he has been with the School of Medicine, Johns Hopkins University, Baltimore, MD, where he is currently serving as a Professor of Biomedical Engineering. He teaches and conducts research on cardiovascular and neurological instrumentation, biomedical signal processing, and micro and nanotechnologies. He has authored more than 150 peer-reviewed publications on these subjects. He has recently established the Center for Neuroengineering at the Johns Hopkins University with the aim of carrying out interdisciplinary and collaborative engineering research for basic and clinical neurosciences. He is actively interested in developing international scientific programs, collaborative exchanges, tutorials and conferences on Neuroengineering and Medical Microsystems.

Dr. Thakor is a recipient of a Research Career Development Award from the National Institutes of Health and a Presidential Young Investigator Award from the National Science Foundation, and is a Fellow of the American Institute of Medical and Biological Engineering, and Founding Fellow of the Biomedical Engineering Society. He is also a recipient of the Centennial Medal from the University of Wisconsin School of Engineering, Honorary Membership from Alpha Eta Mu Beta Biomedical Engineering student Honor Society and Distinguished Service Award from IIT Bombay. He serves on the editorial boards of several journals, including the *Annals of Biomedical Engineering*, IEEE TRANSACTIONS ON BIOMEDICAL ENGINEERING, and IEEE TRANSACTIONS ON INFORMATION TECHNOLOGY IN BIOMEDICINE.